ELSEVIER

Journal of Nuclear Materials 252 (1998) 22–27

journal of nuclear materials

Study of the oxide layer formed on stainless steel exposed to boiling water reactor conditions by ion beam techniques

C. Degueldre [a,*,1], D. Buckley [a], J.C. Dran [b], E. Schenker [a]

[a] *Paul Scherrer Institut (PSI), CH-5232 Villigen, Switzerland*

[b] *CSNSM-CNRS, Laboratoire de recherche des Musées de France, Le Louvre, F-75041 Paris, France*

Received 3 February 1997; accepted 8 October 1997

Abstract

The build-up of the oxide layer on austenitic steel under boiling water reactor (BWR) conditions was studied by macro- and micro-Rutherford backscattering spectrometry (RBS) and sputtered neutral mass spectroscopy (SNMS). RBS is applicable when the oxide thickness is larger than 20 nm and yields both the layer thickness and its stoichiometry. SNMS provides elemental depth profiles and the oxide thickness when combined with profilometry. Stainless steel strip samples pre-treated (electro- or mechanically polished) or not, exposed in a loop simulating the BWR-conditions for periods ranging from 31 to 291 days and with a low water flow velocity show oxide layers with a thickness of about 300 to 600 nm. There is no significant increase of the oxide layer thickness after 31 days of exposure. The paper confirms the presence of inner and outer oxide layers and also confirms the stoichiometry M_2O_3 in the external part in contact with the oxygenated water. The oxide layer consists not only of an outer layer and an inner layer but also of a deep apparent oxide/metal interface that is attributed to oxide formation through the steel grain boundaries. © 1998 Elsevier Science B.V.

1. Introduction

The oxide films formed on stainless steel under boiling water reactor (BWR) conditions need to be fully characterised to understand the mechanisms of corrosion. The morphology and composition of the oxide layer have to be analysed for the different constituent elements and in particular cobalt which produces the largest radiation hazard to personnel from the gamma emitting isotope ^{60}Co [1]. Recent studies rely on the use of sophisticated instrumental analysis such as Auger electron spectrometry (AES) [2] and sputtered neutral mass spectrometry (SNMS) [3]. Recently attention was also drawn to the need of analytical techniques for in situ measurements [4,5]. This information relates to the oxide layer thickness only and more detailed studies are required to better describe the corrosion process and complete previous studies such as that of Maroni et al. [6]. In the present work, the analytical techniques used to characterise the oxide layer are Rutherford backscattering spectrometry (RBS) which has the advantage of being non-destructive and provides information on both the thickness and the stoichiometry of the oxide layer and SNMS depth profile analysis, which provides quantitative data for individual elements.

2. Experimental

A light water reactor simulation loop (LWR-loop) operating at PSI to study the BWR water chemistry with respect to the build-up of oxide on steel surfaces has produced a series of samples for analysis. Since detailed and accurate information is required to model the build-up of the oxide layer on the metal, the loop-exposed samples were analysed by RBS and SNMS to compare results.

* Corresponding author. Fax: +41-56 992 205; e-mail: degueldre@psi.ch.

[1] Also: Department of Analytical Chemistry and Environmental Sciences, University of Geneva.

PII S0022-3115(97)00317-6

Table 1
Standard composition and deliverer's specification of 316 Ti steel as used in this study

	C	Si	Mo	Mn	Cr	Ni	Ti	Co
DIN	< 0.1	< 1.0	2.0–2.5	< 2.0	16.5–18.5	10.5–13.5	> 5C[a]	0.05
Deliverer's specs.	0.041	1.33	2.4	1.33	16.74	10.62	0.36	–

Data in wt%.
[a]Five times the carbon concentration.

2.1. Sample preparation in the loop

2.1.1. Test loop

The loop consists of a feed water unit, a reservoir, a heating and pumping system and test sections with different water flow velocities. The loop is constructed from 316 Ti steel with the composition given in Table 1. The main parameters are: (i) a flow velocity of 0.038 $m\,s^{-1}$ and (ii) an operating temperature of 563 K and a pressure of 9 MPa (90 bar).

The feed water was demineralised by a dual ion exchanger bed followed by a Millipore-filtration system. Organic materials were removed by treating the water with ozone, the excess of ozone was destroyed by irradiation utilising ultra-violet light. The feed water was constantly purged with argon containing sufficient oxygen to attain 400 ppb at the inlet. The inlet water conductivity was $< 0.1\ \mu S\,cm^{-1}$.

2.1.2. Test material and surface finish

The test section contains strips of nuclear grade 316Ti steel, DIN X10CrNiMoTi 18 10: 7 mm width, 1.5 mm thickness. Three different surface finishes were used: 'as delivered', mechanically polished and anodic electropolished. The 'as delivered' and mechanically polished samples, have the same degree of roughness in the order of 0.15 μm (±5%), measured by a Tencor P-2 Long Scan Profiler. The roughness of the anodic electro-polished samples was 0.13 μm.

The strips were exposed in the loop for periods of 31, 97, 180 and 291 days. After exposure, samples were cut from the strips and dried prior to analysis.

2.2. Analytical techniques

2.2.1. Rutherford backscattering spectrometry (RBS)

RBS spectrometry allows rapid analysis of nanometer thick films [7]. The energy of alpha particles backscattered from different constituents of the target is directly related to its elemental composition and their spatial distribution. For a given energy, the alpha particles impinging on the target are scattered by metal (M) atoms, in the case of stainless steel by several elements with similar atomic numbers: iron, nickel and chromium. This produces an edge in the RBS spectrum of the metal the height of which is a function of the atom density. If an oxide layer covers the metal substrate, the density of the alloying elements is reduced. This produces a depression in the RBS spectrum since the scattering power of oxygen is smaller. The deeper the depression in that part of the spectrum due to the metal, the larger the concentration of oxygen in the layer. The wider the depression in the spectrum, the deeper the layer of oxygen atoms extends into the metal alloy and therefore the thicker the oxide film.

RBS was performed on the ARAMIS Tandem Van de Graaff accelerator at CSNSM-CNRS, Orsay. Alpha particles of an incident energy of 2 MeV are backscattered from the samples at an angle of 165°. Samples and standards are mounted on a sample holder disk and placed in the target chamber so that irradiation can be performed with a spatial resolution of 0.1 mm. The incident beam has a diameter of about 1 mm, the information from about 1 mm^2 area reveals the structure of the layer. Calibrations are carried out with an 80 nm gold film on SiO_2 and an aluminium-film on a carbon matrix. The RUMP computer code [8] was used to model the RBS energy spectrum and to determine the oxide layer thickness and stoichiometry by comparing the simulated spectrum with the experimental one. The spectrum modelling was performed considering various assumptions on oxide stoichiometry and thickness. The thicknesses of the layers and their respective stoichiometry, MO_x, are calculated by applying Bragg's law [8] on the basis of the atom density for different components, the stopping cross-sections and an initially assumed thickness. The porosity of the RBS studied material is however not accounted. Unknown thicknesses and stoichiometries were then determined by iterative calculations.

Micro-RBS was performed on the AGLAE Tandem-Van de Graff accelerator [9] at the Laboratoire de Recherche des Musées de France, Le Louvre, Paris. The energy of the alpha particles was 3 MeV and the size of the beam was 3×3 μm. The analysis was performed with a similar backscattering geometry as reported above for the macro analysis. 16 areas were investigated for 4 h. The 16 recorded spectra were displayed separately using a 3D perspective plot for comparison. In addition, a cumulative spectrum was derived.

2.2.2. Sputtered neutral mass spectroscopy (SNMS)

Sputtered neutral mass spectrometry (SNMS) measures neutral species sputtered from the surfaces [10]. The low

pressure and low energy argon plasma eventually erodes a crater through the oxide and into the alloy. The sputtered atoms are ionised by the argon plasma, followed by separation and counting by quadrupole mass spectrometry. SNMS provides elemental depth profiles but as reported for RBS, SNMS does not account for the porosity of the material. The crater size generated by the sputtering is analysed by an independent technique e.g. profilometry.

SNMS-measurements were made at the Alusuisse-Lonza Laboratory in Neuhausen, Switzerland, using a Leybold INA3 unit. The operating parameters were: applied voltage 800 V, which yields a calculated sputtering rate of 1.17 ± 0.10 nm s^{-1} (from the sputtering time and the mean measured values by the profilometer of several crater depths); Ar^+ plasma pressure 4×10^{-6} bar; analysis area in the order of 7 mm^2 ($\approx$ 3 mm diameter). The sputter rate is controlled by the voltage applied to the sample. The quadrupole mass spectrometer was operated in a peak jump mode. This allows tracking of selected elements in a continuous way. The result is an elemental depth profile. The instrument was originally calibrated using an NBS-steel standard.

3. Results

3.1. RBS analysis

As reported earlier [4], the presence of the oxide layer leads to a depression in the RBS spectrum of the sample (Fig. 1). Simulations are carried out by modelling the spectrum either with a constant stoichiometry such as (Fe, Cr, Ni)O_x with x constant over the oxide thickness or with a variable stoichiometry, considering x a function of the film depth.

The recorded spectra present three zones: a first one corresponding to an external layer, a second one corresponding to an internal layer and finally a third one due to an M/MO interface. Actually, RBS considers the external surface flat but the internal interface may be displayed as a relief. A typical RBS-spectrum with the three zones may be modelled considering three stoichiometries. One corresponds to a stoichiometry increase toward a maximum for $x = 1.5$. It is located between two depressions: a first for $x = 1.5$ to 1.3 and a second for x ranging from 1.5 to 0. The maximum stoichiometry of $x = 1.5$ corresponds to an oxide of a M_2O_3 type with a metal to oxygen ratio of 1.5.

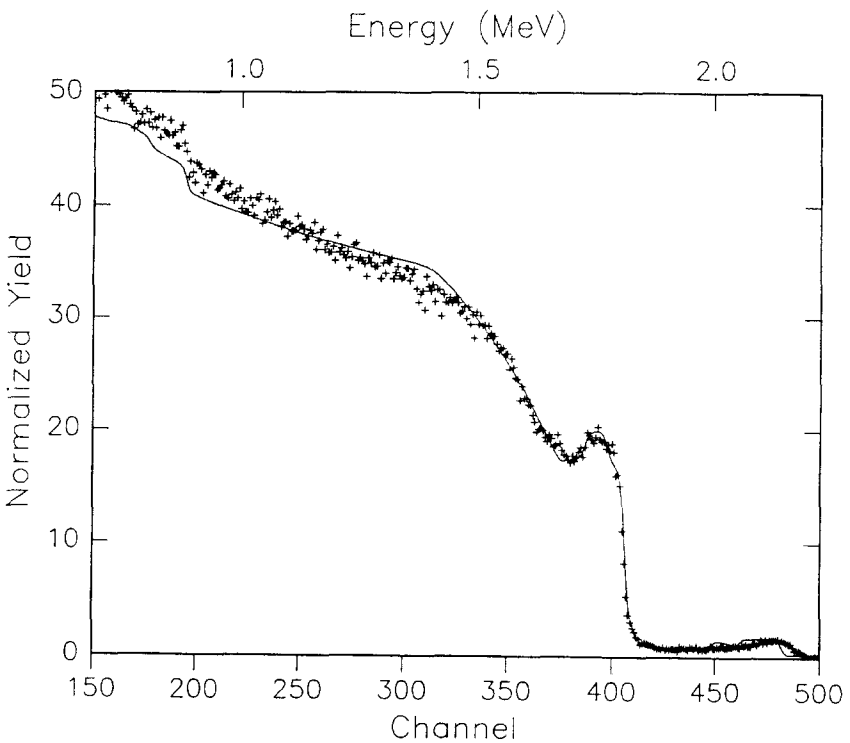

Fig. 1. Typical Macro-RBS spectrum recorded for austenitic stainless steel samples after exposure to the loop water. Conditions: water temperature, 563 K; pressure, 9 MPa (90 bar); water velocity, 0.038 m s^{-1}; 400 ppb O_2; exposure time, 31 days; + experimental counting rate; ———— modeled spectrum. Note the depression in the metal RBS-spectrum due to the oxide layer.

Table 2
Oxide layer thickness measured by RBS and SNMS

Time (days)	Oxide layer thickness (nm)				
	1	2	3	RBS	SNMS
Electropolished samples					
0	5	–	40	5	–
31	150	120	280	270±50	323±13
97	150	120	240	270±50	468±19
180	250	450	800	700±50	491±20
291	250	100	450	350±50	585±23
Mechanically polished samples					
0	5	–	70	5	–
31	150	160	300	310±50	187±7
97	150	140	280	290±50	300±12
180	130	140	280	270±50	284±11
291	130	160	350	290±50	236±9
As delivered samples					
0	5	–	70	5	–
31	120	240	350	360±50	328±13
97	420	240	650	660±50	326±13
180	250	240	650	490±50	397±16
291	150	170	450	320±50	430±17

Conditions: RBS results below 50 nm are uncertain. The layer includes sublayer 1 (external)+sublayer 2 (internal). 3 denotes M/MO interface.

The second to an oxide of the type M_3O_4 with the stoichiometry M/O = 1.33. This maximum in the depression is not always clearly recorded.

The thicknesses of the outer and inner layers as well as of the M/MO interface are given in Table 2. A total layer thickness (inner + outer layer) from the SNMS data is given for comparison. The M/MO layer which relate to the interface relief is not considered in this comparison.

The micro-RBS spectra (Fig. 2) obtained for a sample exposed for 31 days to the loop water are also comparable, demonstrating the homogeneity of the oxide layer after this exposure time. This confirms what was observed on the surface by SEM. Micrographs of the 31 days sample surfaces showed no specific submicroscopic inhomogeneities. Only local microscopic phases (i.e. oxide crystals) are observed for more aged samples (re-crystallisation). The visible roughness increases with the exposure time in the loop.

3.2. SNMS analysis

Fig. 3(a) and (b) presents the depth profile of two samples with different surface finish exposed to the loop water for a period of 31 days. The spectra exhibit a chromium enrichment in the internal layer and evidence of highly oxidised species layer as already discussed by Buckley and Schenker [3]. The depth resolution for a layer of 1 μm is in the order of 5 nm [10]. The data are plotted as sputtering time versus intensity, rather than depth in nanometers, giving the trend of the oxide profile. The oxide thickness for each sample was calculated for the point where a characteristic change in the oxide composition takes place. Starting with the oxide–alloy interface, the depth at this point was calculated first after the data has been smoothed using a fast Fourier smoothing fit. Subsequently, the conventionally used method, calculating the point where the value is half the maximum, $t_{1/2}$, of the elemental concentration has been used, converting the sputtering time to depth using the data from profilometry as previously mentioned. The measured oxide thicknesses are reported in Table 2. The difference of oxide layer thicknesses are occasionally noted because the samples used for SNMS and RBS are not the same, they were prepared in the same conditions but these samples are two different pieces.

Sensitivity tests showed excellent comparison between the sample elemental concentrations and the measured concentrations. The Fe concentration in the steel is 67% and that measured was 70%, while both Ni and Cr concen-

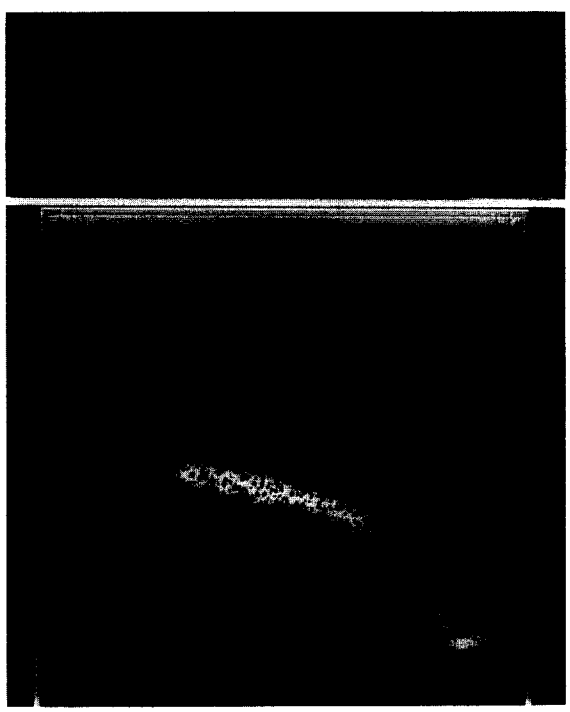

Fig. 2. Micro-RBS spectra recorded for a austenitic stainless steel sample after exposure to the loop water. Conditions: Electropolished stainless steel sample exposed for 31 days to the loop water; for other conditions see Fig. 1. Cumulative spectrum from 16 analyses: note the ^{16}O resonance peak, the marker points to the energy at which the detailed micro-RBS spectra are displayed. The energy window shows: above, white, diffuse sublayer; grey, both internal and external sublayers; below, white, the raising edge (like for metal); bottom, the Mo edge.

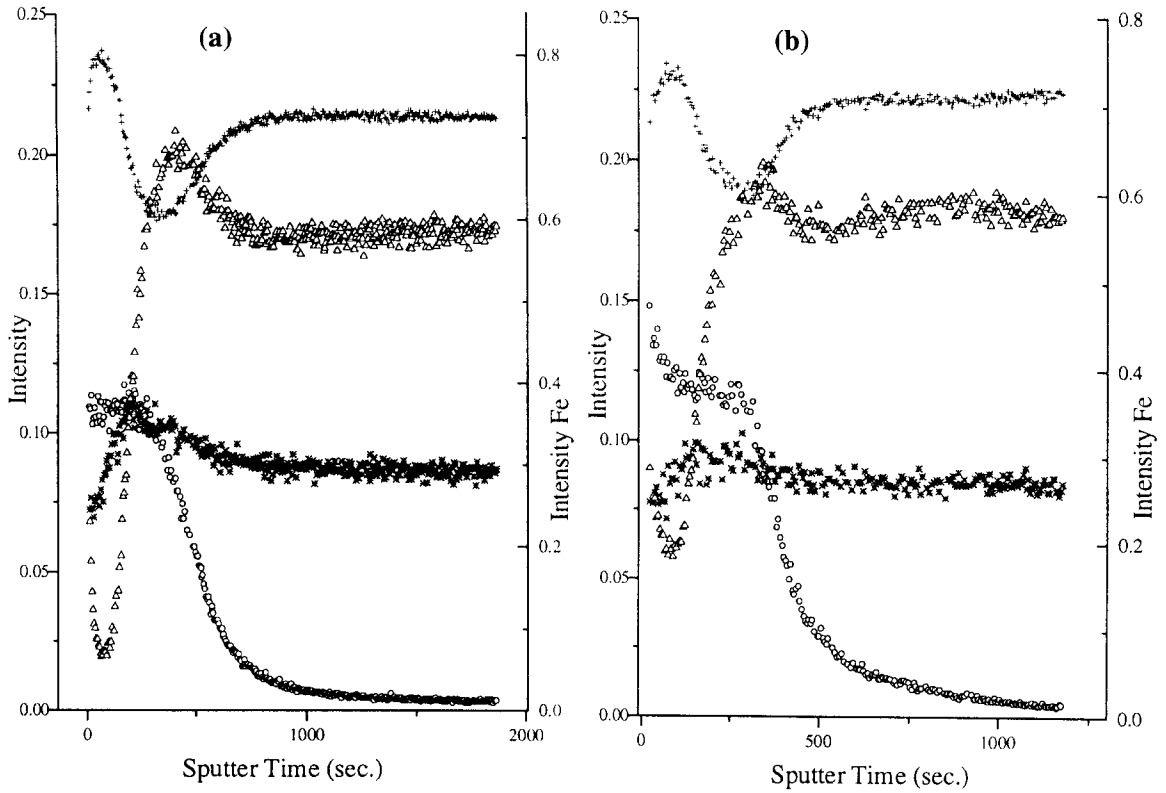

Fig. 3. SNMS depth profile for two samples. Conditions: 31 days of exposure time with a water velocity of 0.038 $m\,s^{-1}$ studied surface finishes: (a) as delivered and (b) electropolished. ○, O; △, Cr; +, Fe; ∗, Ni.

trations were comparable with that given in Table 1 within 1%. Compared with the RBS result, the oxygen profile through the layer makes sense corresponding for the external layer to the expected M_2O_3 stoichiometry.

4. Discussion

The oxide thicknesses determined by RBS and SNMS analyses are compared in Table 2. It is observed that after 31 days of exposure the depth of the oxide layer is hardly influenced by the exposure time in the loop water. The layer thickness is roughly independent of the exposure time and reaches 400 ± 200 nm after 31 days independent of the surface finish. The oxide thickness has reached a steady state which may correspond to the balance between oxide layer build-up and dissolution. The rate of the build-up is limited by cation and oxygen diffusion through the solid film and the porous structure, the rate of the dissolution is limited by the dissolution of the external oxide layer and the diffusion of dissolved species from the internal layer through the pores into the water. This leads to an enrichment of specific species and the formation of an inner and an outer layer. This is explained by Robertson [13] and Tomlison [11] considering the diffusion of species derived from alloy constituents and the permeability of the oxide layer. The surface finish has a marked influence on the oxide structure. 'As delivered' and mechanically polished samples have a more chromium-rich inner layer than the electropolished sample [3], also nickel enrichment was observed toward the outer layer such as for Co [14]. These observations are consistent with the presence of FeCrO, or Cr_2O_3 in the inner layer and $NiFe_2O_4$ or NiO in the outer layer. This may explain the stoichiometry (oxygen to metal ratio) of 1.5 for the inner and 1.33 for the outer layer.

Elemental depth profiles may be explained on the basis of the redox gradient between metal and oxidising water interface. Chromium is depleted in the external layer which is consistent with its oxidation to soluble species, i.e. Cr (VI), but may be enriched near the M/MO interface as Cr(III) species. This result is confirmed by the Fe–Cr–H_2O Pourbaix diagram estimated by Maroni et al. [6] for 300°C showing the stability area of $FeCr_2O_4$, Cr_2O_3 and Fe_2O_3.

The M/MO corrosion interface broadening was earlier observed by AES [2], secondary ion mass spectroscopy [12] and glow lamp discharge spectroscopy [13]. The effect of interface broadening as reported by Yang et al. [2] increases with increased water temperature; this could be

due to pore enlargement. In this work, corrosion interface broadening is recorded for both macro- and micro-RBS as well as for SNMS analysis.

From the RBS analysis it is observed that the oxide on the metal surface has a stoichiometry of 1.5 corresponding to highly oxidised species. It is in the M/MO interface and the thickness ranges from 300 to 800 nm (Table 2). This could be due to a relief effect in the interface oxide/metal or to an intergranular space enlargement by oxide phase formation. Since this layer relates to interface relief, it is not considered in the comparison with the SNMS results.

All the recorded RBS spectra of the 16 investigated microscopic zones present similar profiles, confirming outer and inner layers and a layer corresponding to corrosion interface broadening. The SEM pictures of untreated stainless steel samples show that the austenite crystals have sizes of about 5 m. Since oxygen diffusion into the metal is unlikely for steric reasons, the hypothesis of pore enlargement by oxide phase formation in the intergranular space is consistent with the observations.

The effect of interface broadening reported by Yang et al. [2] increases with increased water temperature. For the single temperature used in this study, the broadening of the oxide/metal interface was observed by both SNMS and RBS analyses. An enhancement of the interface broadening as a function of exposure time was not detected. This is consistent with the postulated mechanism of oxide layer build-up and dissolution as presented by Sanchez et al. [15] or could be due to a passivation.

5. Conclusion

The oxide layer on austenitic stainless steel has been analysed by RBS and SNMS and results, thickness and stoichiometry, are comparable. They confirm the presence of highly oxidised species at the surface followed by medium oxidised phases towards the metal. External and internal layers are built on a metal/oxide interface may be due to oxide formation in the intergranular spaces. Both techniques provide valuable information but are unable to account for the porosity of the layer. This requires the use of microscopic techniques (e.g. TEM). Further corrosion studies should also be performed with the micro-beam techniques (RBS and SIMS) and with large grain (> 50 μm) austenite in order to fully demonstrate this intergranular corrosion effect and with XAFS for completing the fine chemical analysis of the layers.

Acknowledgements

Acknowledgements are due to Dr Alder for his constructive comments, Mr Hirt for his technical assistance, Mr Hamstuts from Alusuisse for SNMS analyses and Mr Salomon for micro-RBS. The Swiss Federal Safety Inspectorate (HSK) is thanked for the financial support.

References

[1] H.P. Alder, D. Buckley, R. Grauer, K. Wiedmann. PSI Report No. 45, 1989.
[2] W. Yang, G. Zhao, M. Zhang, J. Congleton, Corros. Sci. 33 (1992) 89.
[3] D. Buckley, E. Schenker, in: Proc. Int. Conf. La Chimie dans les Reacteurs a Eau, vol. 1, Nice, 24–27 April, 1994, French Nuclear Society, p. 211.
[4] C. Degueldre, J.C. Dran, E. Schenker, J. Nucl. Mater. 188 (1992) 255.
[5] C. Degueldre, S. O'Prey, W. Francioni, Corros. Sci. 38 (10) (1996) 1763.
[6] V. Maroni, C. Melendres, T. Kassner, R. Kumar, S. Siegel, J Nucl. Mater. 172 (1990) 13.
[7] J. Bird, J. Williams, Ion Beam for Material Analysis, Academic Press, New York, 1989.
[8] W. Chu, G. Mayer, M. Nicolet, Backscattering Spectrometry, Academic Press, New York, 1983.
[9] N. Lovestam, T. Calligaro, A. Duval, J. Salomon, Nucl. Instrum. Meth. B 77 (1993) 66.
[10] D. Briggs, P. Seah (Eds.), Practical Surface Analysis, vol. II, 2nd ed., Wiley, New York, 1990.
[11] L. Tomlison, Corrosion 37 (1981) 591.
[12] S. Ono, N. Haginuma, M. Kumagai, K. Tachibana, K. Ishigure, J. Nucl. Sci. Technol. 32 (2) (1995) 125.
[13] J. Robertson, Corros. Sci. 29 (1989) 1275.
[14] C. Lin, F. Smith, R. Cowan, in: Proc. Int. Conf.: La Chimie dans les Réacteurs à Eau, vol. 1, Nice, 24–27 April, 1994, French Nuclear Society, p. 271.
[15] L. Sanchez-Caldera, P. Griffith, E. Rabinovicz, Transact. Am. Soc. Mec. Eng. 110 (1980) 180.